

# Design and Optimization of Copper Antimony Sulfide Thin Film Solar Cell

Sujoy Bhattacharjee <sup>†</sup>, Mehedi Hassan <sup>\*</sup>, N.K. Das <sup>\*</sup>, Mrinmoy Dey <sup>\*</sup>

<sup>\*</sup>Department of Electrical and Electronic Engineering, Chittagong University of Engineering and Technology,  
Chittagong-4349, Bangladesh

(sujoy.cuet@gmail.com, u1602024@student.cuet.ac.bd, nipudas@cuet.ac.bd, mrinmoy@cuet.ac.bd)

<sup>†</sup>

Corresponding Author; Sujoy Bhattacharjee, Department of Electrical and Electronic Engineering, Chittagong University of Engineering and Technology, Chittagong-4349, Bangladesh, Tel: +8801632825831, sujoy.cuet@gmail.com

Received: 12.04.2023 Accepted:08.06.2023

**Abstract-** This research study investigates the prospects of Copper Antimony Sulfide (CuSbS<sub>2</sub>) as an efficient, cost-effective, and thermally stable thin film solar cell. CuSbS<sub>2</sub> is a chalcostibite-based semiconductor absorber that can be used in place of CIGS/CdTe thin film solar cells. CuSbS<sub>2</sub> is a superior absorber alternative because its components are simple, have significant hole mobility, and have a large dielectric constant. Besides, the abundantly available chalcostibite CuSbS<sub>2</sub> has a bandgap of 1.52 eV and an optical absorption coefficient of 10<sup>5</sup> cm<sup>-1</sup>, making it a perfect candidate for a thin film absorber layer. A numerical analysis has been carried out using the wx-AMPS software to evaluate the efficiency and other performance parameters of the proposed CuSbS<sub>2</sub> cell. The optimized cell has a structure of FTO/ZnO/CuSbS<sub>2</sub>/Back contact. A conversion efficiency of 27.29% (FF=86.97%, V<sub>oc</sub>=1.15 V and J<sub>sc</sub>=27.31 mA/cm<sup>2</sup>) and temperature coefficient of -0.0319 %/°C have been found for 2 μm CuSbS<sub>2</sub> absorber layer. Then the effect of BSF on cells stability and performance was analyzed by inserting a SnSe BSF layer in the structure. The designed cell, which has a 100 nm SnSe layer as the BSF and a 2 μm CuSbS<sub>2</sub> absorber, has a higher conversion efficiency of 28.13% (FF=87.18%, V<sub>oc</sub>=1.17 V and J<sub>sc</sub>=27.59 mA/cm<sup>2</sup>) and a better temperature coefficient of -0.0242 %/°C. Based on the results of numerical analysis, CuSbS<sub>2</sub> exhibits excellent potential as an absorber material for solar cell applications.

**Keywords:** Thin film, CuSbS<sub>2</sub>, BSF, PCE, wxAMPS.

## Nomenclature

| Symbols                               |                                   |
|---------------------------------------|-----------------------------------|
| ε <sub>r</sub>                        | Dielectric Relative Permittivity  |
| W (nm)                                | Thickness                         |
| χ (eV)                                | Electron Affinity                 |
| E <sub>g</sub> (eV)                   | Band Gap                          |
| V <sub>oc</sub> (V)                   | Open Circuit Voltage              |
| J <sub>sc</sub> (mA/cm <sup>2</sup> ) | Short Circuit Current             |
| FF                                    | Fill Factor                       |
| N <sub>A</sub> (cm <sup>-3</sup> )    | Acceptor Density                  |
| N <sub>C</sub> (cm <sup>-3</sup> )    | Conduction Band Effective Density |
| N <sub>D</sub> (cm <sup>-3</sup> )    | Donor Density                     |
| N <sub>V</sub> (cm <sup>-3</sup> )    | Valance Band Effective Density    |
| η (%)                                 | Efficiency                        |
| μ <sub>e</sub> (cm <sup>-2</sup> /Vs) | Electron Mobility                 |
| μ <sub>h</sub> (cm <sup>-2</sup> /Vs) | Hole Mobility                     |

|        |             |
|--------|-------------|
| T (°C) | Temperature |
| Ω      | Ohm         |

## Acronyms and Abbreviations

|        |   |
|--------|---|
| BSF    | Back Surface Field                                  |
| TCO    | Transparent Conductive Oxide                        |
| FTO    | Florine Tin Oxide                                   |
| ZnO    | Zinc Oxide  |
| CAS    | Copper Antimony Sulfide                             |
| SnSe   | Tin Selenide  |
| wxAMPS | Analysis of Microelectronic and Photonic Structured |
| TFSC   | Thin Film Solar Cell                                |
| PCE    | Photo Conversion Efficiency                         |
| TC     | Temperature Coefficient                             |

## 1. Introduction

Chalcostibite ( $\text{CuSbS}_2$ ), a comparatively little-known ternary I-V-VI<sub>2</sub> chalcogenide, is being explored as a potential photo-absorber for numerous reasons. Both theoretical calculations and actual studies show that  $\text{CuSbS}_2$  has a direct band gap of 1.38-1.5 eV [1]-[3], which is in the optimum absorber layer band gap range. According to a recent study,  $\text{CuSbS}_2$  can absorb light in a range of 350-900 nm [4], and the absorption coefficient increases by more than  $10^4 \text{ cm}^{-1}$  over the band gap energy of 1.5 eV [5]. CAS's bandgap and optical absorption make it an ideal absorber layer material. To a considerable degree, none of the constituents that go into the production of  $\text{CuSbS}_2$  are dangerous to human health, and all of them are easily accessible and inexpensive. Because of its non-toxicity and relative abundance,  $\text{CuSbS}_2$  can be utilized as an alternative to CIGS, CdTe, and CZTS.

For the synthesis of copper antimony sulfide ( $\text{CuSbS}_2$ ), researchers used a number of direct and indirect approaches. Both physical and chemical approaches have been used to create CAS thin films, resulting in a variety of characteristics. Thermal evaporation, co-sputtering, spin coating, electro deposition and Chemical Bath Deposition are some of the approaches. Due to the lack of sophisticated instrumentation and a vacuum system, chemical bath deposition (CBD) is a relatively less expensive thin-film fabrication technique [6]. Another inexpensive and straightforward method for thin layer deposition is chemical spray pyrolysis [7]. A thermal evaporation technique was utilized to fabricate  $\text{CuSbS}_2$  on a clean glass substrate [8]-[9].  $\text{CuSbS}_2$  thin films were formed as a result of co-RF sputtering of  $\text{Sb}_2\text{S}_3$  and  $\text{Cu}_2\text{S}$  targets. By adjusting  $\text{Sb}_2\text{S}_3$  flow and substrate temperature, the carrier concentration of the phase pure  $\text{CuSbS}_2$  film could be adjusted [10]. Although the manufacturing of CAS-based solar cells has yet to be attempted, this developing photoactive material is understudied.  $\text{CuSbS}_2$  thin films were created by spin coating Cu-Sb-S stock solution onto FTO-coated substrates and then annealing them in multiple steps, as described by Yang et al. in 2014 [11]. The photo conversion efficiency of the structure was 0.5%. According to Welch et al., cells made by co-sputtering  $\text{Sb}_2\text{S}_3$  and  $\text{Cu}_2\text{S}$  exhibited an efficiency of 0.86 percent [12]. Septina et al. developed structure by stacking Cu/Sb metal layers and sulfurizing them at high temperatures under  $\text{H}_2\text{S}$  flow which provides 3% photo conversion efficiency [13]. M. Pal et al. used SCAPS-1D simulation software to design a cell structure with  $\text{CuSbS}_2$  absorber that yielded an efficiency of 10.71% [14]. However, the most efficient cell structure in the numerical study was reported by S. Das et al., whose proposed cell structure Mo/p- $\text{CuSbS}_2$  (3  $\mu\text{m}$ )/n- $\text{TiO}_2$ /ZnO:Al/ITO provided 28.06% photo conversion efficiency [15].

The wxAMPS simulation software was utilized to perform a numerical analysis in order to study the potential of CAS as an alternative absorber layer material. The ideal heterojunction partner and TCO layer for the suggested absorber layer material have been identified through a comparative analysis. The PCE of solar cells is reduced because of back surface recombination that occurs at the semiconductor (p-type absorber)/metal contact interface. The

addition of the BSF layer creates a barrier to the minority carrier's access to the back surface and directs the minority carrier's (electrons) motion toward the depletion region, acting as an electron reflector. The BSF technique has been successfully used in improving the performance characteristics of solar cells in AISb [16], GaAs [17], CdTe [18], CZTS [19], CIGS [20] and 2D materials [21]-[22] based solar cells. In this study, the impact of the back surface field (BSF) layer on the performance of  $\text{CuSbS}_2$  solar cells was evaluated, and suggested an optimal BSF layer for the solar cell structure. Furthermore, thermal stability assessments at various stages were conducted, which enabled the calculation of the temperature coefficient. Finally, a novel cell structure was proposed, with each layer's parameters meticulously optimized to create a more efficient and thermally stable solar cell configuration.

## 2. Modeling and Simulation

In the development of any optoelectronics structure, the contact properties play a crucial role. After proper optimization, a structure is proposed in order to determine the potential of solar cells. A photovoltaic solar cell is intended to convert the maximum amount of sunlight into electricity. In order to successfully construct a solar cell, it is essential to pick the appropriate TCO, window layer, and absorber layer. It is impossible to achieve maximum conversion efficiency without minimizing optical losses. In order to improve the optimal structure, various factors must be taken into account. The method of simulating a genuine phenomenon by using a collection of mathematical formulae is the foundation upon which simulation software is built. Widespread use of simulation software in the design of machinery ensures that the end result will be as near to the original design specifications as is feasible without the need for costly process modifications. Software based on numerical simulation is utilized to observe the behavior and performance of solar cells.

In this research study, the numerical simulation was carried out using wx-AMPS software. The wxAMPS software is a revised version of the widely-used AMPS tool for simulating solar cells [23-24]. The wxAMPS software is a high-performance tool for simulating the characteristics of different heterojunction solar cell structures. It boasts a convenient user interface and incorporates both the intra-band and the trap-assisted tunneling model. A novel algorithm that utilizes the Newton and Gummel techniques has been developed to improve the convergence characteristic of a program. Additionally, this algorithm renders the modeling of intra-band tunneling effects feasible for heavy-recombination devices [25]. The integration of Matlab's robust coding capabilities with the adaptable wxAMPS console version enables the feasibility of conducting batch simulations for solar cells [26]. Fig. 1 illustrates the construction of the TFSC structure that was used for this research. The p-type  $\text{CuSbS}_2$  light absorption layer is part of the general device structure, together with an n-type window layer, a front transparent conducting oxide, and a BSF layer. The proposed structure is

(FTO/ZnO/CuSbS<sub>2</sub>/SnSe/Back contact) presented in Fig.1. The CuSbS<sub>2</sub> absorber layer thickness was changed from 0.1 μm to 5 μm and optimized at 2 μm with a PCE of 27.29%. Thin-film solar cells' transparent conductive oxide layer is a heavily doped n-type semiconductor material with a larger band gap than other layers. For the TCO layer, conductive oxide-type materials are often utilized, and this study chose FTO as the material. The excellent visible transparency of FTO is attributed to its wide bandgap and low electrical resistivity [27]. The next layer is n-type ZnO window layer having a bandgap of 3 eV. For the window layer, the material should be chosen so that most of the incoming photons are transmitted to the absorber. ZnO has recently gained popularity as a window layer material due to its high transparency across the entire visible spectral range, higher mobility for electron, and stability [9]. Due to high transparency, it passes most of the incident photon towards the CuSbS<sub>2</sub> absorber layer. This particular kind of solar cell has a broad spectrum of losses. The BSF technology provides assistance in the process of optimizing the structure. As a result, a BSF layer of SnSe is added to the CAS solar cell to further increase its performance, and its impact on the modified cell structure is investigated. Without adequate solar radiation, solar cells do not perform optimally [28]-[29]. The photovoltaic cell parameters were measured using the wx-AMPS software at AM 1.5G sun spectrum and 300 K temperature.

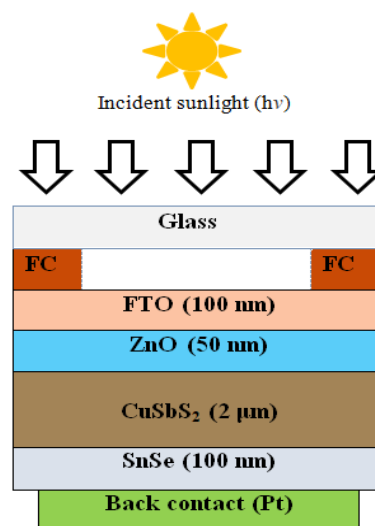


**Fig. 1.** Proposed structure of CuSbS<sub>2</sub> cell

Material characteristics employed in this modeling study were collected from published values [15], [30]–[32], and acceptable estimation at few cases. Table 1 shows the properties of the materials utilized.

**Table 1.** Simulation parameters for wx-AMPS software

| Parameter                             | FTO                  | n-ZnO                 | p-CuSbS <sub>2</sub>   | p-SnSe                 |
|---------------------------------------|----------------------|-----------------------|------------------------|------------------------|
| W (μm)                                | 0.1                  | 0.05                  | 0.1-5                  | 0.1                    |
| ε <sub>r</sub>                        | 10                   | 9                     | 14.6                   | 17                     |
| E <sub>g</sub> (eV)                   | 3.5                  | 3                     | 1.52                   | 1.3                    |
| N <sub>c</sub> (cm <sup>-3</sup> )    | 2×10 <sup>18</sup>   | 2×10 <sup>18</sup>    | 2×10 <sup>18</sup>     | 2.2× 10 <sup>18</sup>  |
| N <sub>v</sub> (cm <sup>-3</sup> )    | 1.8×10 <sup>19</sup> | 1.5× 10 <sup>19</sup> | 1×10 <sup>19</sup>     | 1.78× 10 <sup>19</sup> |
| μ <sub>n</sub> (cm <sup>2</sup> /v/s) | 100                  | 100                   | 49                     | 25                     |
| μ <sub>p</sub> (cm <sup>2</sup> /v/s) | 20                   | 25                    | 49                     | 89                     |
| N <sub>a</sub> (cm <sup>-3</sup> )    | 0                    | 0                     | 1.38× 10 <sup>18</sup> | 3×10 <sup>18</sup>     |
| N <sub>d</sub> (cm <sup>-3</sup> )    | 1×10 <sup>18</sup>   | 1×10 <sup>17</sup>    | 0                      | 0                      |
| χ (eV)                                | 4.5                  | 4.5                   | 3.85                   | 4.35                   |

### 3. Results and Discussion

#### 3.1. Impact of Window Layer on Cell Performance

The window layer works with the absorber layer as a hetero-junction partner ensuring the optimum value is kept. High transparency and low resistivity are required window layer properties [33, 34], so that incident photon can pass through this layer with minimal loss and reach the absorbent layer. A comparative study of various p-n structures was carried out. Among these, ZnO has demonstrated the best performance.

The optimal value of the window has been selected by adjusting the thickness of the window layer. In Fig. 2, the thickness of the window layer varies from 20 nm to 100 nm. As shown in the graph,  $J_{sc}$  and  $\eta$  decrease with increasing thickness. For practical purposes, thicknesses below 50 nm are not considered. Since a thicker window layer increases bulk resistance, the overall performance also suffers; the thickness of the window layer has been adjusted to 50 nm.

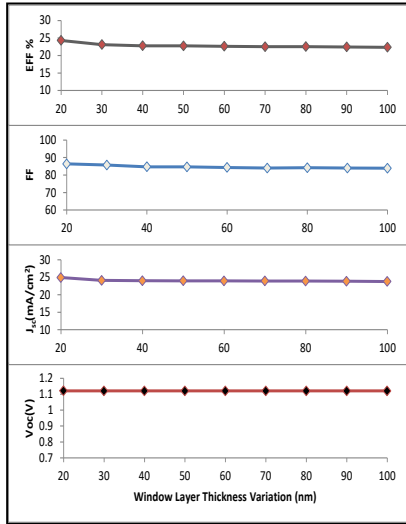


**Fig. 2.** ZnO Window Layer Thickness Optimization

**3.2. Impact of TCO Layer on Cell Performance**

Low thickness, high transmittance, and a relatively higher band gap than any other solar device materials are necessary conditions for TCO material. In order to enhance effective electron transport, the TCO layer materials must be able to create good contact with the metallic grid. This is an essential requirement for the layer. Since an n-n+ junction makes quasi-ohmic contact with the contact grid, allowing electrons to move laterally towards the contact grid, the overall concentration of the TCO layer material should be as high as possible. The electrical conductivity of TCO must be sufficiently high while minimizing optical absorption losses [35]. TCOs typically have a large optical band gap (generally larger than 3.0 eV) to enable the passage of light with a low resistivity value of around  $10^{-4} \Omega\text{-cm}$  [33]. FTO is employed as a TCO layer in the proposed structure.

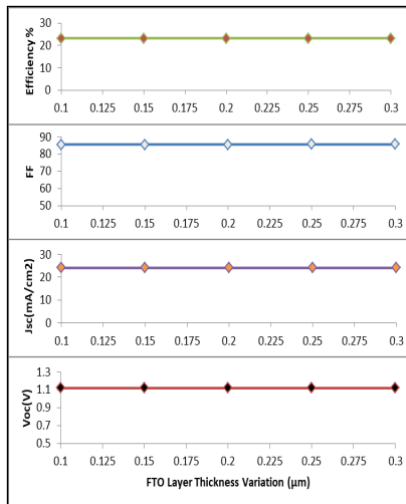


**Fig. 3.** FTO as TCO layer Thickness Optimization

**3.3. CuSbS<sub>2</sub> Absorber Layer Thickness Variation**

The absorber layer thickness in Fig. 4 ranges from 20 nm to 5 µm. The graph shows that  $V_{oc}$ ,  $J_{sc}$ , FF, and efficiency all go

up as the thickness keeps increasing. It has enabled the collection of longer wavelengths of illumination, which has aided in the production of Electron Hole Pairs. Consequently, the value of  $V_{oc}$  and  $J_{sc}$  has increased. The absorber layer thickness has been optimized at 2 µm, with 27.29% efficiency. According to Fig. 4, the efficiency improves as the thickness increases, but the other performance parameters reach their maximum value. To preserve the material, the absorber layer has been kept at 2 µm.

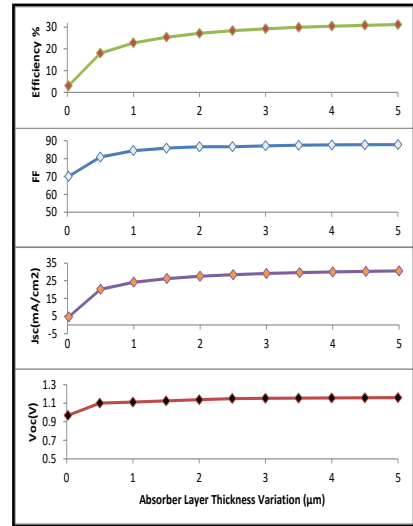


**Fig. 4.** Absorber Layer Thickness Optimization

As shown in Fig. 5,  $J_{sc}$  has significantly improved while  $V_{oc}$  has remained nearly constant as the thickness is increased from 1 µm to 2 µm. Because of the accumulation of longer wavelengths of light, a greater short circuit current is generated by more electron hole pairs.

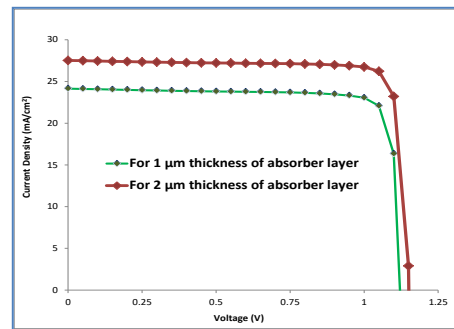


**Fig. 5.** J-V curve comparison before and after optimizing absorber layer thickness

**3.4. CuSbS<sub>2</sub> Absorber Doping Concentration Variation**

Up to a certain point, a rise in doping concentration improves cell performance measures. The doping concentration of the CuSbS<sub>2</sub> absorber is varied from  $1 \times 10^{13} \text{ cm}^{-3}$  to  $1 \times 10^{19} \text{ cm}^{-3}$  range. Up to a point, increasing the doping concentration improves cell performance. It can be observed in Fig. 6, that  $V_{oc}$ , FF and  $\eta$  have increased with the increase of doping concentration, while  $J_{sc}$  has remained almost constant. From the total observation and based on previous

experiments  $1.38 \times 10^{18}$  doping concentration of the absorber is chosen for the perfect operation.

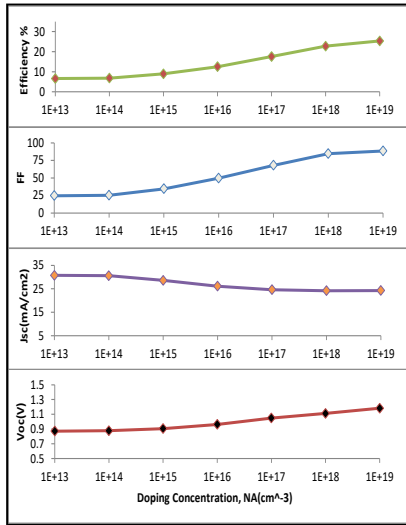


**Fig. 6.** Doping Concentration Variation of the Absorber Layer

3.5. Insertion of SnSe BSF

Carrier recombination at the rear surface of an ultrathin absorber decreases cell performance due to a shorter carrier lifetime. Additionally, some incident photons will be lost in the vicinity of back contact materials, reducing the carrier production rate even further. Back Surface Field (BSF) is one technique that produces an electric field to force minority carrier electrons toward the front contact zone by reflecting them in the rear surface area [36].

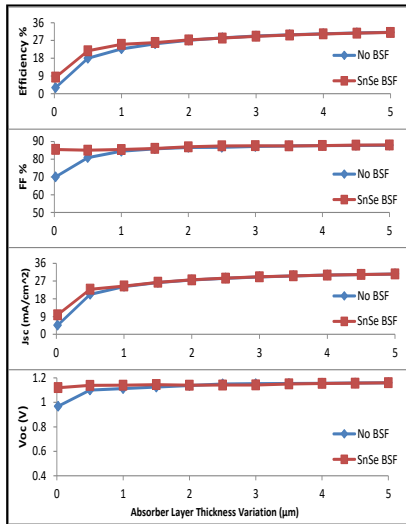


**Fig. 7.** Cell performance characteristics for the change of absorber layer thickness in the modified cell with and without SnSe BSF

A SnSe BSF layer was added to the optimized cell structure. Following the selection of the BSF material, the thickness of the CuSbS<sub>2</sub> absorber layer is then tuned in order to produce a model cell that is both cost-effective and thin. During the

simulation, all of the layer thicknesses were kept at the same values as those of the optimized structure. However, the thickness of the CuSbS<sub>2</sub> layer was changed from 200 nm to 5 µm, and an additional BSF layer of SnSe was added. The impacts of varied thicknesses of the CuSbS<sub>2</sub> absorber layer are shown in Fig. 7, along with their respective effects on the performance parameters of the cell, both with and without the presence of the BSF. It is clear from examining Fig. 7 that the BSF is operable with an ultrathin absorber layer. According to Fig. 7, the BSF layer works efficiently with less than a 2 µm thick absorber layer. An SnSe BSF layer of 100 nm thickness improves the efficiency of the structure from 27.29% to 28.13%

The doping concentration of p-CuSbS<sub>2</sub> was varied from  $1 \times 10^{13} \text{ cm}^{-3}$  to  $1 \times 10^{19} \text{ cm}^{-3}$  to evaluate the performance metrics of both the cell structure optimized with and without the BSF layer. Through simulation, the performance of cell parameters under higher doping concentrations was investigated, and the result is illustrated in Fig. 8.

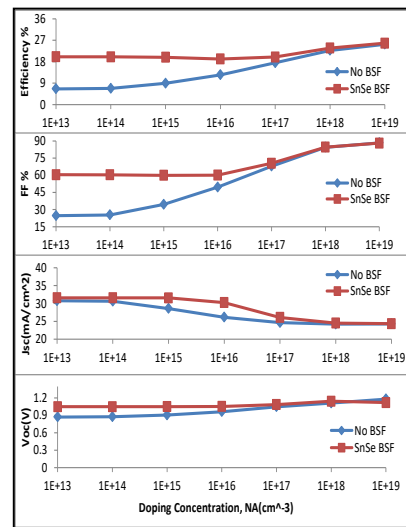


**Fig. 8.** Cell performance characteristics for the change of absorber layer doping concentration in the optimized cell with and without SnSe BSF

According to Fig. 7, the BSF layer works efficiently with less than a 2 µm thick absorber layer. An SnSe BSF layer of 100 nm thickness improves the efficiency of the structure from 27.29% to 28.13%.

3.6. Temperature Variation of Optimized Cell Structure

Solar cells, similar to other semiconductor devices, are temperature dependent. With increasing temperature, the bandgap of semiconductor materials reduces, leading to a notable decrease in open circuit voltage and a slight increase in short-circuit current. Consequently, solar cell performance deteriorates as the temperature rises. Fluctuations in operating temperature contribute to variations in the cell's parameter performance, as highlighted by previous studies [37]-[38]. An investigation of the thermal stability of the suggested cell is carried out in order to examine the potential of the CuSbS<sub>2</sub> absorber layer.

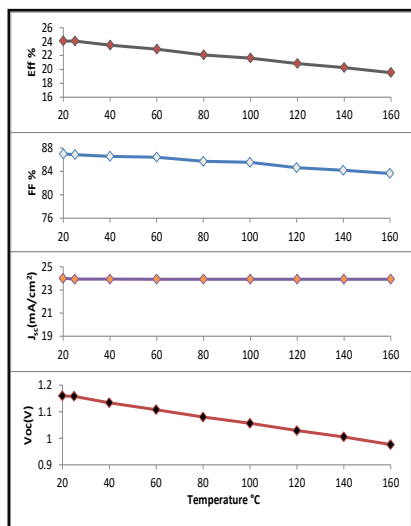


**Fig. 9.** Temperature Variation of the Optimized Structure

Fig. 9 makes it very evident that, according to what one would anticipate, the performance deteriorates as the temperature rises. This is because the energy band gap becomes unstable at higher temperatures, which speeds up the rate at which electrons and holes recombine. In order to evaluate the performance of the cell, it is necessary to make a comparison between the performance characteristics of a

suggested modified cell and those of a conventional structure. So, the performance of the cell structure with and without the BSF layer is compared at a variety of operating temperatures, and the comparative simulation results for both cells are shown in Fig. 10.

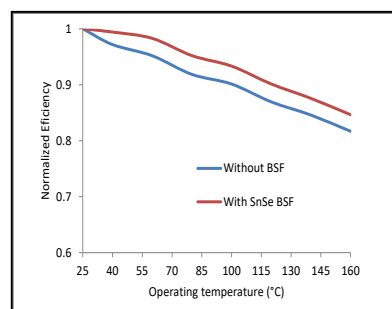


**Fig. 10.** Changes in operating temperature and their effects on normalized efficiency

The efficiency has reduced in a linear fashion in conjunction with the temperature, with  $TC = -0.0319 \text{ \%}/^\circ\text{C}$  for the cell without BSF and  $TC = -0.0242 \text{ \%}/^\circ\text{C}$  for the suggested cell with SnSe BSF. The thermal stability of the suggested cell that uses SnSe BSF is superior to that of the cell that does not use BSF.

**Table 2.** Performance Comparison of 2 Device Structures

| Structure                      | FTO/ZnO/CuSbS <sub>2</sub> / Back contact (Mo) | FTO/ZnO/CuSbS <sub>2</sub> / SnSe/ Back contact (Mo) |
|--------------------------------|--|--|
| $V_{oc}$ (V)                   | 1.15   | 1.17   |
| $J_{sc}$ (mA/cm <sup>2</sup> ) | 27.31  | 27.59  |
| FF (%)                         | 86.97  | 87.18  |
| PCE (%)                        | 27.29  | 28.13  |
| TC (%/°C)                      | -0.0319  | -0.0242  |

#### 4. Conclusion

A TFSC structure with a non-toxic, low-cost CuSbS<sub>2</sub> absorber was devised and optimized. The highest conversion efficiency of 28.13% (FF=87.18%,  $V_{oc}$ =1.17 V and  $J_{sc}$ =27.59 mA/cm<sup>2</sup>) was obtained with 2 μm thick absorber layer along with 100 nm of SnSe BSF. The optimized structure without SnSe BSF provided 27.29% (FF=86.97%,  $V_{oc}$ =1.15 V and  $J_{sc}$ =27.31 mA/cm<sup>2</sup>) of photo conversion efficiency. In terms of thermal stability, the modified cell with the BSF layer performed noticeably better than the cell without BSF. The findings demonstrate that a highly efficient ultra-thin solar cell composed of CuSbS<sub>2</sub> can be created.

#### References

[1] J. Zhou, G. Q. Bian, Q. Y. Zhu, Y. Zhang, C. Y. Li, and J. Dai, "Solvothermal crystal growth of CuSbQ<sub>2</sub> (Q=S, Se) and the correlation between macroscopic morphology

and microscopic structure," *J. Solid State Chem.*, vol. 182, no. 2, pp. 259–264, 2009, doi: 10.1016/j.jssc.2008.10.025.

[2] Y. Rodríguez-Lazcano, M. T. S. Nair, and P. K. Nair, "Cu<sub>x</sub>Sb<sub>y</sub>S<sub>z</sub> thin films produced by annealing chemically deposited Sb<sub>2</sub>S<sub>3</sub>-CuS thin films," *Mod. Phys. Lett. B*, vol. 15, no. 17–19, pp. 667–670, Aug. 2001, doi: 10.1142/S0217984901002257.

[3] W. Shockley and H. J. Queisser, "Detailed balance limit of efficiency of p-n junction solar cells," *J. Appl. Phys.*, vol. 32, no. 3, pp. 510–519, 1961, doi: 10.1063/1.1736034.

[4] S. Dekhil, H. Dahman, S. Rabaoui, N. Yaacoub, and L. El Mir, "Investigation on microstructural and optical properties of CuSbS<sub>2</sub> nanoparticles synthesized by

- hydrothermal technique,” *J. Mater. Sci. Mater. Electron.*, vol. 28, no. 16, pp. 11631–11635, 2017, doi: 10.1007/s10854-017-6965-8.
- [5] D. J. Temple, A. B. Kehoe, J. P. Allen, G. W. Watson, and D. O. Scanlon, “Geometry, electronic structure, and bonding in  $\text{CuMCh}_2$  (M = Sb, Bi; Ch = S, Se): Alternative solar cell absorber materials?,” *J. Phys. Chem. C*, vol. 116, no. 13, pp. 7334–7340, 2012, doi: 10.1021/jp300862v.
- [6] C. Macías, S. Lugo b, Á. Benítez, I. López, B. Kharissov, A. Vázquez, and Y. Peña, “Thin film solar cell based on  $\text{CuSbS}_2$  absorber prepared by chemical bath deposition (CBD),” *Mater. Res. Bull.*, vol. 87, 2017, doi: 10.1016/j.materresbull.2016.11.028.
- [7] S. Manolache, A. Duta, L. Isac, M. Nanu, A. Goossens, and J. Schoonman, “The influence of the precursor concentration on  $\text{CuSbS}_2$  thin films deposited from aqueous solutions,” *Thin Solid Films*, vol. 515, no. 15 SPEC. ISS., pp. 5957–5960, 2007, doi: 10.1016/j.tsf.2006.12.046.
- [8] A. Hussain, R. Ahmed, N. Ali, F. K. Butt, A. Shaari, W.N. Wan Shamsuri, R. Khenata, D. Prakash, and K.D. Verma “Post annealing effects on structural, optical and electrical properties of  $\text{CuSbS}_2$  thin films fabricated by combinatorial thermal evaporation technique,” *Superlattices Microstruct.*, vol. 89, pp. 136–144, 2016, doi: 10.1016/j.spmi.2015.10.024.
- [9] M. Dey, N. K. Das, M. Dey, S. F. U. Farhad, M. A. Matin, and N. Amin, “Impact of Source to Substrate Distance on the Properties of Thermally Evaporated CdS Film,” *Int. J. Renew. Energy Res.*, vol. 11, no. 1, pp. 495–503, 2021, doi: 10.20508/ijrer.v11i1.11627.g8168.
- [10] B. Krishnan, S. Shaji, and R. Ernesto Ornelas, “Progress in development of copper antimony sulfide thin films as an alternative material for solar energy harvesting,” *J. Mater. Sci. Mater. Electron.*, vol. 26, no. 7, pp. 4770–4781, 2015, doi: 10.1007/s10854-015-3092-2.
- [11] B. Yang., L. Wang, J. Han, Y. Zhou, H. Song, S. Chen, J. Zhong, L. Lv, D. Niu, and J. Tang “ $\text{CuSbS}_2$  as a Promising Earth-Abundant Photovoltaic Absorber Material: A Combined Theoretical and Experimental Study,” no. iii, 2014.
- [12] A. W. Welch, P. P. Zawadzki, S. Lany, C. A. Wolden, and A. Zakutayev, “Self-regulated growth and tunable properties of  $\text{CuSbS}_2$  solar absorbers,” *Sol. Energy Mater. Sol. Cells*, vol. 132, pp. 499–506, 2015, doi: 10.1016/J.SOLMAT.2014.09.041.
- [13] W. Septina, S. Ikeda, Y. Iga, T. Harada, and M. Matsumura, “Thin film solar cell based on  $\text{CuSbS}_2$  absorber fabricated from an electrochemically deposited metal stack,” *Thin Solid Films*, vol. 550, pp. 700–704, 2014, doi: 10.1016/j.tsf.2013.11.046.
- [14] E. Puente-López and M. Pal, “Numerical simulation and optimization of physical properties for high efficiency  $\text{CuSbS}_2$  thin film solar cells,” *Optik (Stuttg.)*, vol. 272, p. 170233, Feb. 2023, doi: 10.1016/J.IJLEO.2022.170233.
- [15] S. Das and A. Beltran, “High Efficiency non-toxic  $\text{CuSbS}_2$ -based Heterojunction Solar Cell with  $\text{TiO}_2$  Electron Transport Layer,” *Conf. Rec. IEEE Photovolt. Spec. Conf.*, pp. 1876–1879, 2019, doi: 10.1109/PVSC40753.2019.8981380.
- [16] M. Dey, R. Chakma, N. Rahman, M. Dey, N.K. Das, A. K. S. Gupta, M. A. Matin, N. Amin “Study of ultra-thin and stable  $\text{AlSb}$  solar cell with potential copper telluride BSF,” *5th IEEE Reg. 10 Humanit. Technol. Conf. 2017, R10-HTC 2017*, vol. 2018-Janua, no. December, pp. 811–814, 2018, doi: 10.1109/R10-HTC.2017.8289079.
- [17] K. J. Singh and S. K. Sarkar, “Highly efficient ARC less  $\text{InGaP/GaAs}$  DJ solar cell numerical modeling using optimized  $\text{InAlGaP}$  BSF layers,” *Opt. Quantum Electron.*, vol. 43, no. 1–5, pp. 1–21, 2012, doi: 10.1007/s11082-011-9499-y.
- [18] M. Dey, M. A. Matin, N. K. Das, and M. Dey, “Germanium telluride as a BSF material for high efficiency ultra-thin  $\text{CdTe}$  solar cell,” 2014, doi: 10.1109/IFOST.2014.6991134.
- [19] Y. H. Khattak, F. Baig, H. Toura, S. Ullah, B. Marí, S. Beg, and H. Ullah “Effect of CZTSe BSF and minority carrier life time on the efficiency enhancement of CZTS kesterite solar cell,” *Curr. Appl. Phys.*, vol. 18, no. 6, pp. 633–641, 2018, doi: 10.1016/j.cap.2018.03.013.
- [20] S. Benabbas, H. Heriche, Z. Rouabah, and N. Chelali, “Enhancing the efficiency of CIGS thin film solar cells by inserting novel back surface field ( $\text{SnS}$ ) layer,” *2014 North African Work. Dielectr. Mater. Photovolt. Syst. NAWDMPV 2014*, no. August, 2014, doi: 10.1109/NAWDMPV.2014.6997611.
- [21] M. Dey, M. F. Shahriar, A. Ali, M. Dey, and N. K. Das, “Design and Optimization of an Efficient Molybdenum Disulfide ( $\text{MoS}_2$ ) Solar cell with Tin Sulfide BSF,” 2019, doi: 10.1109/ECACE.2019.8679178.
- [22] J. He, T. Zhao, X. Jing, and N. A. O. Demerdash, “Application of wide bandgap devices in renewable energy systems - Benefits and challenges,” 2014, doi: 10.1109/ICRERA.2014.7016485.
- [23] Y. Liu, Y. Sun, and A. Rockett, “A new simulation software of solar cells -  $\text{WxAMPS}$ ,” *Sol. Energy Mater. Sol. Cells*, vol. 98, pp. 124–128, 2012, doi: 10.1016/j.solmat.2011.10.010.
- [24] A. C. Busacca, V. Rocca, L. Curcio, A. Parisi, A. C. Cino, R. Pernice, A. Andò, G. Adamo, A. Tomasino, G. Palmisano, S. Stivala, M. Caruso, G. Cipriani, D. La Cascia, V. Di Dio, G. R. Galluzzo, R. Miceli “Parametrical study of multilayer structures for CIGS solar cells,” 2014, doi: 10.1109/ICRERA.2014.7016528.
- [25] Y. Liu, D. Heinzl, and A. Rockett, “A new solar cell simulator:  $\text{WxAMPS}$ ,” *Conf. Rec. IEEE Photovolt. Spec. Conf.*, pp. 002753–002756, 2011, doi: 10.1109/PVSC.2011.6186517.
- [26] Y. Liu, Y. Sun, and A. Rockett, “Batch simulation of solar cells by using Matlab and  $\text{wxAMPS}$ ,” *Conf. Rec. IEEE*

- Photovolt. Spec. Conf.*, pp. 902–905, 2012, doi: 10.1109/PVSC.2012.6317748.
- [27] K. Subba Ramaiah and V. Sundara Raja, “Structural and electrical properties of fluorine doped tin oxide films prepared by spray-pyrolysis technique,” *Appl. Surf. Sci.*, vol. 253, no. 3, pp. 1451–1458, 2006, doi: 10.1016/j.apsusc.2006.02.019.
- [28] R. Z. Caglayan, K. Kayisli, N. Zhakiyev, A. Harrouz, and I. Colak, “A review of hybrid renewable energy systems and MPPT methods,” *Int. J. Smart Grid-ijSmartGrid*, vol. 6, no. 3, pp. 72–78, 2022.
- [29] M. R. Rashel, A. Albino, M. Tlemcani, T. C. F. Goncalves, J. Rifath, and A. Hasan, “MATLAB Simulink modeling of photovoltaic cells for understanding shadow effect,” 2017, doi: 10.1109/ICRERA.2016.7884434.
- [30] Z. Liang, Q. Zhang, O. Wiranwetchayan, J. Xi, Z. Yang, K. Park, C. Li, and G. Cao “Effects of the morphology of a ZnO buffer layer on the photovoltaic performance of inverted polymer solar cells,” *Adv. Funct. Mater.*, vol. 22, no. 10, pp. 2194–2201, 2012, doi: 10.1002/adfm.201101915.
- [31] A. D. Adewoyin, M. A. Olopade, and M. A. C. Chendo, “A comparative study of the effect of transparent conducting oxides on the performance of  $\text{Cu}_2\text{ZnSnS}_4$  thin film solar cell,” *J. Comput. Electron.*, vol. 17, no. 1, pp. 361–372, 2018, doi: 10.1007/s10825-017-1106-4.
- [32] E. M. K. Ikbali Ahamed, S. Bhowmik, M. A. Matin, and N. Amin, “Highly efficient ultra thin  $\text{Cu}(\text{In}, \text{Ga})\text{Se}_2$  solar cell with Tin Selenide BSF,” *ECCE 2017 - Int. Conf. Electr. Comput. Commun. Eng.*, pp. 428–432, 2017, doi: 10.1109/ECACE.2017.7912942.
- [33] Y. W. Heo, Y. W. Heo, D. P. Norton, L. C. Tien, Y. Kwon, B. S. Kang, F. Ren, S. J. Pearton, and J. R. Laroche “ZnO nanowire growth and devices,” *Mater. Sci. Eng. R Reports*, vol. 47, no. 1–2, pp. 1–47, 2004, doi: 10.1016/j.mser.2004.09.001.
- [34] M. S. White, D. C. Olson, S. E. Shaheen, N. Kopidakis, and D. S. Ginley, “Inverted bulk-heterojunction organic photovoltaic device using a solution-derived ZnO underlayer,” *Appl. Phys. Lett.*, vol. 89, no. 14, pp. 87–90, 2006, doi: 10.1063/1.2359579.
- [35] Z. Remes, M. Vanecsek, H. M. Yates, P. Evans, and D. W. Sheel, “Optical properties of  $\text{SnO}_2\text{:F}$  films deposited by atmospheric pressure CVD,” *Thin Solid Films*, vol. 517, no. 23, pp. 6287–6289, 2009, doi: 10.1016/j.tsf.2009.02.109.
- [36] O. Von Roos and O. Von Roos, “A simple theory of back surface field (BSF) solar cells,” vol. 3503, no. 1978, 2012, doi: 10.1063/1.325262.
- [37] A. H. Shiravi and M. Firoozzadeh, “Performance assessment of a finned photovoltaic module exposed to an air stream: an experimental study,” *J. Brazilian Soc. Mech. Sci. Eng.*, vol. 44, no. 11, 2022, doi: 10.1007/s40430-022-03832-0.
- [38] F. Javed, “Impact of Temperature & Illumination for Improvement in Photovoltaic System Efficiency,” *Int. J. Smart grid*, vol. 6, no. v6i1, 2022, doi: 10.20508/ijsmartgrid.v6i1.222.g185.